

## **Data-driven gross patient motion detection and compensation: Implications for coronary <sup>18</sup>F-NaF PET imaging**

Martin Lyngby Lassen<sup>1</sup>, Jacek Kwiecinski<sup>1,2</sup>, Sebastien Cadet<sup>1</sup>, Damini Dey<sup>1</sup>, Chengjia Wang<sup>2</sup>, Marc R Dweck<sup>2</sup>, Daniel S Berman<sup>1</sup>, Guido Germano<sup>1</sup>, David E Newby<sup>2</sup>, Piotr J Slomka<sup>1</sup>

<sup>1</sup>Cedars-Sinai Medical Center, Los Angeles, CA, USA

<sup>2</sup>British Heart Foundation Centre for Cardiovascular Science, Clinical Research Imaging Centre, Edinburgh Heart Centre, University of Edinburgh, Edinburgh, United Kingdom

Keywords: Data-driven motion detection, Motion compensation, Cardiac PET, PET/CT

Words: 4967/5000

Corresponding Author: Piotr J Slomka, PhD

Artificial Intelligence in Medicine Program

Cedars-Sinai Medical Center

8700 Beverly Blvd Ste A047N

Los Angeles, California 90048 USA

[piotr.slomka@cshs.org](mailto:piotr.slomka@cshs.org)

First Author: Martin Lyngby Lassen, PhD

Artificial Intelligence in Medicine Program

Cedars-Sinai Medical Center

8700 Beverly Blvd Ste A047N

Los Angeles, California 90048 USA

[Martinlyngby.lassen@cshs.org](mailto:Martinlyngby.lassen@cshs.org)

Short running title: Data-driven GPM detection and correction

## **ABSTRACT**

Patient motion degrades image-quality, affecting the quantitative assessment of PET-images. This affects studies of coronary lesions where micro-calcification processes are targeted. Coronary PET imaging protocols require up to 30-min scans, introducing the risk of gross patient motion (GPM) during the acquisition. Here, we investigate the feasibility of an automated data-driven method for detection of GPM during the PET-acquisition.

### **Methods**

Twenty-eight patients with stable coronary disease underwent a 30-min PET acquisition 1 hour after injection of  $248 \pm 10$  MBq  $^{18}\text{F}$ - Sodium Fluoride (NaF), followed by a coronary computed tomography angiography (CTA) scan. An automated data-driven GPM detection technique tracking the center-of-mass (CoM) of the count rates for every 200 milliseconds in the PET list-mode data was devised and evaluated. Two patient motion patterns were considered: sudden repositioning (motion  $>0.5$  mm within 3 seconds) and general repositioning (motion  $>0.3$  mm over 15 seconds or more). After reconstruction of diastolic images, individual GPM frames with focal coronary uptake were co-registered in 3D, creating a GPM-compensated (GPMC) image series.

Lesion motion was reported for all lesions with focal uptake. Relative differences in maximum standard uptake value ( $\text{SUV}_{\text{max}}$ ) and target to background ratio (TBR) between GPMC and non-GPMC (standard electrocardiogram gated data) diastolic PET images were compared in three separate groups defined by the maximum motion observed in the lesion ( $<5$ , 5-10 and  $>10$  mm).

## Results

A total of 35  $^{18}\text{F}$ -NaF-avid lesions were identified in 28 patients. An average of  $3.5 \pm 1.5$  GPM frames were considered for each patient, resulting in an average frame duration of  $7 \pm 4$  (range, 3 – 21) min. Mean per-patient motion was:  $7 \pm 3$  mm (maximum 13.7 mm). GPMC increased  $\text{SUV}_{\text{max}}$  and TBR in all lesions with motion  $>5$  mm. Lesions with 5-10 mm motion (N=15) had  $\text{SUV}_{\text{max}}$  and TBR increased by  $4.6 \pm 5.6\%$  ( $p=0.02$ ) and  $5.8 \pm 6.4\%$  ( $p<0.002$ ) respectively; lesions with motion  $\geq 10$  mm (N=15) had  $\text{SUV}_{\text{max}}$  and TBR increased by  $5.0 \pm 5.3\%$  ( $p=0.009$ ) and  $11.5 \pm 10.1\%$  ( $p=0.001$ ) respectively. GPM correction led to diagnostic reclassification of 3 (11%) patients.

## Conclusion

GPM during coronary  $^{18}\text{F}$ -NaF PET-imaging is common and may affect the quantitative accuracy. An automated retrospective compensation of this motion is feasible and should be considered for coronary PET imaging.

## INTRODUCTION

Motion-related artifacts are detrimental to quantitative PET-imaging. Three different motion patterns have been identified for the thoracic region; cardiorespiratory motion as well as gross patient motion (GPM). Different strategies have been proposed to identify and correct for the induced motion. In clinical practice, 3-lead electrocardiogram are routinely used for cardiac gating (1). Several strategies for respiratory motion detection have been proposed, using either external markers or data-driven approaches (1–3). Respiratory motion is often corrected using either gating approaches or through dedicated motion compensation techniques (3–6). Several techniques have been proposed for neurological PET-scans (7,8), however GPM has not been investigated thoroughly for thoracic imaging protocols.

The impact of GPM is of interest in many thoracic PET-imaging protocols (9). One application is coronary plaque imaging protocol, which is affected by all three above-mentioned motion patterns. These imaging studies target the identification of lesions with active calcification processes, which have been linked to unstable coronary atherosclerotic plaques (10–13). Unfortunately, the lesions are often of the same size as the spatial resolution of the PET-component in most modern PET/CT systems (50-500 mm<sup>3</sup>) which hampers their identification (14). Several motion limiting and dedicated correction techniques for the cardiorespiratory motion have been proposed to obtain quantitative accurate assessments of the tracer-uptake in the lesions (12,15–17). Nevertheless, GPM might impair the full potential of both respiratory and cardiac compensation techniques not only for coronary plaque studies, but all thoracic imaging protocols.

In this work, we aimed to estimate the frequency and relative impact of GPM on image quality in a patient cohort examined for coronary artery disease using  $^{18}\text{F}$ -sodium fluoride ( $^{18}\text{F}$ -NaF). To this end, we developed a general, retrospective PET data-driven GPM detection for bulk motion on thoracic PET. The proposed GPM detection and compensation method is applicable without the need for modifying the standard imaging acquisition protocols, as all motion detection events are based on the already existing PET listmode data.

## MATERIALS AND METHODS

### Study Population

This study population is comprised of 28 patients who underwent hybrid  $^{18}\text{F}$ -NaF PET/CT examinations of the coronary arteries (*Table 1*). All patients had angiographically confirmed multivessel coronary artery disease defined as either a stenosis ( $> 50\%$ ) or previous revascularization. Exclusion criteria included renal dysfunction (estimated glomerular filtration rate  $\leq 30$  mL/min/1.73 m<sup>2</sup>), contraindication to CT-contrast agents and acute coronary syndrome within 12 months prior to the examination. This study was approved by the local investigational review board (Edinburgh, UK) and written informed consent was obtained from all subjects.

### Imaging Protocol

*PET/CT.* Patients were injected with  $(248\pm 10)$  MBq  $^{18}\text{F}$ -NaF tracer approximately one-hour prior ( $71\pm 16$  min) to a 30-minute PET acquisition in list-mode format, performed on a 128-slice Biograph mCT system (Siemens Healthineers, Knoxville, USA). All patients were scanned with arms positioned above the head. A low-dose CT for attenuation correction purposes prior to the PET-emission acquisition (120 kV, 50 mAs, 3 mm slice thickness) was obtained immediately before PET imaging. All patients were acquired using tracking for cardiac contractions using 3-lead electrocardiogram, without additional tracking of respiratory motion using external devices.

*CT angiography.* A coronary CT angiography (CTA) was acquired immediately following the PET acquisition for anatomical identification of the lesions. The CTA was performed with prospective gating, 330 milliseconds rotation time, body-mass index (BMI)

dependent voltage (BMI <25, 100 kV; BMI ≥25, 120 kV), tube-currents of 160-245 mAs. The patients had administered beta-blockers (orally or intravenously) to achieve a target heart-rate of <60 beats/min. A BMI-dependent bolus-injection of contrast media (400 mg/mL) was administered to the patients with a flow of 5-6 mL/s after determining the appropriate trigger delay with a test bolus of 20 mL contrast material.

### **Image reconstruction**

Two different PET datasets were evaluated in this study, a diastolic frame (3<sup>rd</sup> gate from standard 4-gate electrocardiogram gated reconstruction) without GPM compensation (non-GPMC), as utilized in the original coronary <sup>18</sup>F-NaF PET study (12), and the same diastolic frame with GPM compensated (GPMC) image-series (See sections: “GPM detection” and “GPM correction”).

Both (GPMC and non-GPMC) datasets were reconstructed using the Siemens UltraHD reconstruction algorithm, which corrects for point-spread function and time-of-flight (18). The images were reconstructed in batch-mode using 2 iterations, 21 subsets, followed by a 3D 5-mm Gaussian filtration using the vendor-provided reconstruction toolbox (e7 tools (JSRecon12), Siemens Healthineers, Knoxville, TN).

### **GPM detection**

Information on patient repositioning events was extracted from the acquired PET-list data using an automated data-driven projection-based GPM detection technique. The detection of the GPM was based on evaluations of the center-of-mass (CoM) (Equation 1) of single-slice rebinned sinograms (the rebinning algorithm compress the full 3D

sinogram to a series of 2D sinograms (3D volume)), with assessments for every 200 ms of the acquired list file (2,19).

$$CoM(t) = \frac{\sum_i i \cdot T(i,t)}{\sum_i T(i,t)} \quad (1)$$

Where  $T$  is the histogram for the time segment  $t$  and  $i$  the slice number of the obtained counts (Figure 1, B). Each CoM assessment provided a position in the single-slice rebinned sinogram with three components (x, y and z), corresponding to a radial, angular and axial position, respectively. While shifts of the z-component (axial motion) can be translated from the sinogram space to motion observed in the images are translations between shifts in the transaxial plane to the angular/radial plane not straight forward. Despite the non-obvious connection between the motion measured in sinogram space and actual motion in image-space, it is still possible to detect even complex motion patterns such as cardiac contractions (2).

Two kinds of GPM were considered from the CoM assessments: (1) sudden repositioning (SR), most likely due to sudden patient discomfort (Figure 1A), and (2) gradual patient motion (GR) (Figure 1A, green, red, dark blue, orange and bright blue boxes, respectively), characterized by a general drift in the CoM baseline occurring as a result of general muscle relaxation during the acquisition. SR-events were considered when sudden changes in the CoM baseline assessment of more than 0.5 mm were detected within a time interval of 3 seconds (Figure 1). Likewise, GR events were defined as general drifts of the CoM baseline exceeding 0.3 mm over a time interval spanning >15 seconds.

Owing to the general properties of the used method, which previously have been used to detect respiratory motion, the respiratory motion is embedded in the CoM

baseline assessment (2,20,21). The respiratory motion has a normal oscillating frequency of 0.2-0.5 Hz (12-30 respiratory cycles per minute), which permit filtering of respiratory frequencies, such that only the underlying GPM component is present for the subsequent assessments. In the current study, the raw CoM-baseline data was filtered using a band-stop filter (bandwidth 0.2-0.5 Hz). Following the band-stop filtering, the GPM signal was filtered using a moving average filter (3 seconds) to minimize the effect of residual noise in the signal introduced by deep breath-holds or shallow breathing (Figure 1). Frames with duration <3 min were excluded from the following data-assessment to ensure sufficient counting statistics in the resulting GPMC images.

### **GPM compensation**

The motion compensation technique consisted of three steps, delineation of the lesions, followed by the definition of the reference frame, and finally, image co-registration.

*Delineation:* Myocardial lesions with focal uptake were identified on the non-GPMC PET-images based on common features in the two image-series (presence of signal in CTA, and focal uptake in the PET images). All identified lesions were subject to a threshold-based delineation of the lesion (70% of  $SUV_{max}$  in the lesion) using a cylindrical volume.

*Reference frame definition:* The reference frame was defined as the GPM frame with the lowest sum of square differences (most similar frame) in comparison to the non-GPMC image (Figure 2).

*Image co-registration:* The subsequent image co-registration was obtained through local measures of the motion vector fields, obtained through delineations of the

lesions. In this study, the lesions were segmented in an in-house developed software (FusionQuant) using a spherical volume of interest (VOI) ( $r = 5$  mm) enclosing the part of the lesion with the highest uptake in the reference frame. The corresponding part of the lesion was segmented for all subsequent GPM frames. To preserve the outline as well as the heterogeneity of the lesions were the delineated lesions co-registered using a rigid 3-parameter translation using the center-of-mass assessment of the delineated lesions as the objective function. Through the co-registrations, we obtained a gross patient motion compensated image.

### **Image analysis**

*Patient motion.* The magnitude of GPM was evaluated across patients. Patient motion was assessed in 3D (in mm) by calculation of the motion vectors obtained during the co-registration process. Average and maximum per lesion motion was reported in 5-min intervals. In addition, the per-lesion motion was evaluated using three motion intervals ( $<5$ , 5-10, and  $\geq 10$  mm respectively).

*Effect of GPM on quantitative measures.* Based on anatomical references obtained from the CTA images, 3D spherical VOI's (radius 5mm) were placed over the lesions. The VOI's were placed on lesions within all coronary segments with a  $>25\%$  stenosis and a diameter  $\geq 2$  mm. Background blood pool activity was determined by a cylindrical VOI (radius=10 mm, length=15 mm), placed in the right atrium at the level of the takeoff of the right coronary artery. Maximum standard uptake values ( $SUV_{max}$ ) in the VOIs, as well as target-to-background ratios (TBR), were obtained. TBR values were calculated by

dividing the  $SUV_{max}$  of the lesions by the mean SUV obtained from the blood pool ( $SUV_{Background}$ ) of the right ventricle (Equation 2) (22).

$$TBR = \frac{SUV_{max}}{SUV_{Background}} \quad (2)$$

*Diagnostic evaluation.* Two categories of lesions were defined using a previously validated methodology (11,12). In brief,  $^{18}F$ -NaF-avid lesions were identified as lesions with  $TBR \geq 1.25$ , while  $^{18}F$ -NaF-negative lesions had  $TBR < 1.25$ . In this study, we evaluated the effect of the GPM compensation for lesions with focal uptake. GPMC and non-GPMC images were compared by percent-wise increase of the  $SUV_{max}$  and TBR.

### **Statistical analysis**

The data were tested for normality using the Shapiro-Wilk test. The data were presented as mean $\pm$ SD (standard deviation) or median. Image parameters before and after GPM compensation were compared using paired *t*-tests. The statistical analyses were performed in MatLab (MatLab, Mathworks, USA). A two-sided  $P < 0.05$  was considered statistically significant.

## RESULTS

### GPM detection

A total of 35 lesions were identified in 28 non-GPMC patient scans (Table 1). The subjects were found to reposition (SR and GR combined) a total of 110 times during the acquisitions, resulting in an average of 3.9 GPM's per patient. Sixteen (SR = 4, GR = 12) of the 110 GPM frames were discarded due to short frame duration (average duration:  $1.0 \pm 1.0$  min).

The 94 accepted frames resulted in 2 to 7 GPM frames (average  $3.4 \pm 1.2$ ) per patient, corresponding to an average duration of  $8.5 \pm 4$  (range 3-21) min per frame. The GR motion was most common, accounting for 87 of the 94 accepted GPM detections (93%).

### Patient motion

Average lesion translations for each GPM event for lesions with focal uptake were of magnitude  $5.9 \pm 2.8$  mm (Figure 3A). Analyses of per lesion motion in 5-min intervals revealed the most frequent repositioning events in the 10<sup>th</sup> to 15<sup>th</sup> minute interval, with a total of 27 translations during this time period (Figure 3A). Analyses of maximum per patient motion revealed that the patient moved most towards the end of the scan (last 10 min of the acquisition, Figure 3B).

### Quantification

The  $SUV_{max}$  and TBR values increased by  $4.7 \pm 5.8\%$  ( $SUV_{max}$ ,  $p=0.0001$ ) and  $8.4 \pm 8.6\%$  (TBR,  $p<0.0001$ ) on GPMC compared to non-GPMC image (Table 2). Figure 4

displays an example of a patient with an SR-event starting at minute 6 (red enclosure). The patient likely experienced discomfort during the scan, which led to lowering of the arms for 3 min (Figure 4, red enclosure) before the arms were elevated again. The GPM compensation led to 0.4 increase in the  $SUV_{max}$  (corresponding to an increase of 38.6%) and a corresponding increase in the TBR of 0.2, corresponding to an increase of 11%.

In Figure 5, we show an example with large patient motion, which led to shifting of the lesion by more than 1 cm (maximum motion = 11.7 mm). GPMC images show increased  $SUV_{max}$  (21.6% increase) and TBR (20.0% increase) as compared to non-GPMC images.

In another case example, GPMC images show TBR increase of 40% and a corresponding increase in the  $SUV_{max}$  of 20% (Figure 6). This patient had an average motion of  $5.7 \pm 4.1$  mm (maximum = 7.5 mm), leading to a shift of the entire lesion twice during the acquisition. The GPM compensation resulted in a reclassification of the NaF-negative lesion in non-GPMC images (TBR = 1.19) to an NaF-avid lesion in the GPMC image-series (TBR = 1.68).

Increased  $SUV_{max}$  and TBR were reported for all lesions on GPMC images, with most effect on lesions with translations >10 mm (Table 3, Figure 7). The GPM compensation resulted in a reassessment of the lesions in 3 patients (11%), leading to the definition of 38  $^{18}F$ -NaF avid lesions, in contrast to 35 lesions prior to GPM compensation.

## DISCUSSION

In this study, we evaluated the frequency and relative effect of GPM during thoracic PET acquisitions, and motion compensation for these events. Our main finding holds that patient repositioning events occur approximately 3-4 times during the 30-min acquisition on the average. The proposed GPM compensation approach could increase the  $SUV_{max}$  and TBR by up to 30 and 40%, respectively, and led to the reclassification of  $^{18}F$ -NaF lesions in three patients (11%) with lesions becoming  $^{18}F$ -NaF-avid despite initially being perceived as  $^{18}F$ -NaF-negative. We demonstrate a simple, but effective automated data-driven patient motion compensation technique which utilizes exclusively list-mode data, does not require any additional hardware during image acquisition, and can be applied retrospectively to data obtained with standard protocols.

To date, GPM during image acquisition has been explored primarily for neurological imaging where hardware solutions based on infra-red systems and MR-based navigators have been proposed (7,8). Unfortunately, these techniques cannot easily be adapted for cardiovascular imaging in PET/CT systems due to the complex motion patterns of the myocardium, and the need for additional advanced hardware. Alternatively, data-driven methods (PET-only based) evaluating the patient positioning during the acquisition have proven their ability to accurately identify respiratory motion during the acquisition (2,23,24). As demonstrated in our study, these techniques could also be used for the detection of GPM during the acquisition when a steady tracer distribution during the scan time can be assumed.

In addition, the proposed GPM detection method is not restricted purely to coronary lesion imaging, as no anatomical identifiers were used in the CoM assessment of the patient. The proposed technique evaluates the CoM of the acquired PET list-file data, which has the same distribution of counts as observed in non-attenuation corrected PET-images. As GPM events shift the entire thorax, it is inevitable that the shifts in the high-uptake areas such as lung and skin, as seen in non-attenuation corrected PET-images, do not change the CoM assessment. For this reason, the method, although based on a CoM-based approach may benefit from the heterogeneous sensitivity profile observed in the PET-system (24). The bulk motion events will introduce shifts in the observed countrates, used for the GPM detection, which might amplify the detection of the repositioning events. Owing to these effects, it is likely that the proposed detection technique can detect repositioning events regardless of the underlying morphological changes in the body and the tracer used for the assessment.

The GPM compensation approach has several important implications for the clinical assessment of vulnerable plaques in the coronary  $^{18}\text{F}$ -NaF PET imaging protocols. Coronary PET image-quality is hampered by several factors, including respiratory and cardiac motion as well as partial volume effects. Our proposed technique introduces a first-step solution to reduce the consequences of complex GPM patterns during the scan. The implementation presented in this study relies on a relatively simple motion compensation technique based on tracking the lesion signal on time-frames. Nonetheless, GPM compensation may be introduced either before or during image-reconstruction, as shown for studies of respiratory motion compensation (5). These

techniques may combine compensations for GPM and respiratory motion as well as cardiac contraction, into a fully motion-compensated image (12,15,17).

We acknowledge the limitations of this study. This study focused on compensating for motion only in lesions with focal uptake patterns due to the signal void in the negative PET lesions. The observed effect on SUV is modest in some cases, which may be explained by the lack of remaining corrections for respiratory motion as well as partial volume effects. Moreover, only diastolic phase PET images were used to compare GPMC and non-GPMC images in this study. Potentially cardiac-motion compensated images could be also evaluated for GPM (15,16). The proposed GPM detection technique assumes no tracer distribution changes between isolated image frames, which limits its use to scans acquired after steady-state distribution of the tracer. The requirements of the stable tracer-distribution should not affect coronary plaque imaging or most oncological assessments, where the scans often are acquired typically one-hour post injection. Another limitation is the non-linear relationship between the detected motion in the sinogram space and the motion observed in the patient in the reconstructed images. This discrepancy prevents detection of the actual patient motion in mm directly in the sinogram space, which might be necessary in settings where motion compensation during the image-reconstruction is desired. This limitation is, however, not affecting the reporting of the patient motion nor the motion compensation in the current project as these were both obtained in image-space. Finally, the study-population included in this study consisted of only 28 patients, nevertheless the quantitative differences between GPMC and non-GPMC images are statistically significant despite this limited number of patients.

## **CONCLUSION**

Patient motion during thoracic PET protocol leads to reduced TBR and SUV. A simple, yet effective, technique based on a center-of-mass assessment of the raw PET data in listmode format permits reliable detection and compensation for GPM. TBR values were increased in patients with lesion motion exceeding 5 mm, in some cases leading to reclassification of identified lesions. Therefore, GPM compensation should be performed in thoracic PET studies.

## **ACKNOWLEDGEMENTS**

This research was supported in part by grant R01HL135557 from the National Heart, Lung, and Blood Institute/National Institute of Health (NHLBI/NIH). The content is solely the responsibility of the authors and does not necessarily represent the official views of the National Institutes of Health. The study was also supported by a grant (“Cardiac Imaging Research Initiative”) from the Miriam & Sheldon G. Adelson Medical Research Foundation. DEN is supported by the British Heart Foundation (CH/09/002, RM/13/2/30158, RE/13/3/30183) and is the recipient of a Wellcome Trust Senior Investigator Award (WT103782AIA). MRD is supported by the Sir Jules Thorn Biomedical Research Award (JTA/15) and the British Heart Foundation (FS/14/78/31020). We also thank Spencer Zaid (Cedars-Sinai Medical Center) for proofreading the paper. Drs. Berman, Germano and Slomka have received royalties from Cedars-Sinai Medical Center. No other potential conflicts of interest relevant to this article exist.

## REFERENCES

1. Kesner AL, Schleyer PJ, Büther F, Walter MA, Schäfers KP, Koo PJ. On transcending the impasse of respiratory motion correction applications in routine clinical imaging – a consideration of a fully automated data driven motion control framework. *EJNMMI Phys*. 2014;1:8.
2. Büther F, Dawood M, Stegger L, et al. List mode-driven cardiac and respiratory gating in PET. *J Nucl Med*. 2009;50:674-681.
3. Polycarpou I, Tsoumpas C, Marsden PK. Analysis and comparison of two methods for motion correction in PET imaging. *Med Phys*. 2012;39:6474.
4. Slomka PJ, Rubeaux M, Le Meunier L, et al. Dual-gated motion-frozen cardiac PET with Flurpiridaz F18. *J Nucl Med*. 2015;56:1876-1881.
5. Feng T, Wang J, Fung G, Tsui B. Non-rigid dual respiratory and cardiac motion correction methods after, during, and before image reconstruction for 4D cardiac PET. *Phys Med Biol*. 2015;61:151-168.
6. Tsoumpas C, Polycarpou I, Thielemans K, et al. The effect of regularization in motion compensated PET image reconstruction: a realistic numerical 4D simulation study. *Phys Med Biol*. 2013;58:1759-1773.
7. Olesen OV, Paulsen RR, Højgaard L, Roed B, Larsen R. Motion tracking for medical imaging: a nonvisible structured light tracking approach. *IEEE Trans Med Imaging*. 2012;31:79-87.
8. Keller SH, Hansen C, Hansen C, et al. Sparsely sampled MR navigators as a

- practical tool for quality control and correction of head motion in simultaneous PET/MR. *EJNMMI Phys.* 2015;1:A36.
9. Woo J, Tamarappoo B, Dey D, et al. Automatic 3D registration of dynamic stress and rest <sup>82</sup>Rb and flurpiridaz F 18 myocardial perfusion PET data for patient motion detection and correction. *Med Phys.* 2011;38:6313-6326.
  10. Joshi N V, Vesey A, Newby DE, Dweck MR. Will 18F-Sodium Fluoride PET-CT imaging be the magic bullet for identifying vulnerable coronary atherosclerotic plaques? *Curr Cardiol Rep.* 2014;16:14-20.
  11. Dweck MR, Chow MW, Joshi N V, et al. Coronary arterial 18F-sodium fluoride uptake: a novel marker of plaque biology. *J Am Coll Cardiol.* 2012;59:1539-1548.
  12. Joshi N V, Vesey AT, Williams MC, et al. 18F-fluoride positron emission tomography for identification of ruptured and high-risk coronary atherosclerotic plaques: a prospective clinical trial. *Lancet.* 2014;383:705-713.
  13. Cocker MS, Spence JD, Hammond R, et al. [18F]-NaF PET/CT identifies active calcification in carotid plaque. *JACC Cardiovasc Imaging.* 2017;10:486-488.
  14. Motoyama S, Ito H, Sarai M, et al. Plaque characterization by coronary computed tomography angiography and the likelihood of acute coronary events in mid-term follow-up. *J Am Coll Cardiol.* 2015;66:337-346.
  15. Rubeaux M, Joshi N V, Dweck MR, et al. Motion correction of 18F-NaF PET for imaging coronary atherosclerotic plaques. *J Nucl Med.* 2016;57:54-59.
  16. Rubeaux M, Joshi N, Dweck MR, et al. Demons versus level-set motion

- registration for coronary 18 F-sodium fluoride PET. In: Proc SPIE Int Soc Opt Eng. ; 2016:97843Y.
17. Cal-González J, Tsoumpas C, Lassen ML, et al. Impact of motion compensation and partial volume correction for 18F-NaF PET/CT imaging of coronary plaque. *Phys Med Biol.* 2017;63:15005.
  18. Lois C, Jakoby BW, Long MJ, et al. An assessment of the impact of incorporating Time-of-Flight information into vlinical PET/CT imaging. *J Nucl Med.* 2010;51:237-245.
  19. Daube-Witherspoon ME, Muehllehner G. Treatment of axial data in three-dimensional PET. *J Nucl Med.* 1987;28:1717-1724.
  20. Büther F, Ernst I, Dawood M, et al. Detection of respiratory tumour motion using intrinsic list mode-driven gating in positron emission tomography. *Eur J Nucl Med Mol Imaging.* 2010;37:2315-2327.
  21. Bundschuh RA, Martínez-Moeller A, Essler M, et al. Postacquisition detection of tumor motion in the lung and upper abdomen using list-mode PET data: a feasibility study. *J Nucl Med.* 2007;48:758-763.
  22. Pawade TA, Carlidge TRG, Jenkins WSA, et al. Optimization and reproducibility of aortic valve 18F-Fluoride positron emission tomography in patients with aortic stenosis. *Circ Cardiovasc Imaging.* 2016;9:1-11.
  23. Lassen ML, Cal-Gonzalez J, Rasul S, Hacker M, Beyer T. Feasibility of an automated, data-driven respiratory motion compensation: applications to 18F-

FDG myocardial viability patients. *J Nucl Med.* 2016;57:1959.

24. He J, O'Keefe GJ, Gong SJ, et al. A novel method for respiratory motion gated with geometric sensitivity of the scanner in 3D PET. *IEEE Trans Nucl Sci.* 2008;55:2557-2565.

**Table 1:** Baseline characteristics and demographics of the 28 patients

|                                    |          |
|------------------------------------|----------|
| <b>Demographics</b>                |          |
| Age (years)                        | 68.5±8.7 |
| Gender (Males / Females)           | 26 / 2   |
| Body-mass Index (BMI)              | 25.8±3.0 |
| <b>Cardiovascular risk factors</b> |          |
| Diabetes Mellitus                  | 0        |
| Current Smoker                     | 3        |
| Hypertension                       | 21       |
| Hyperlipidemia                     | 28       |

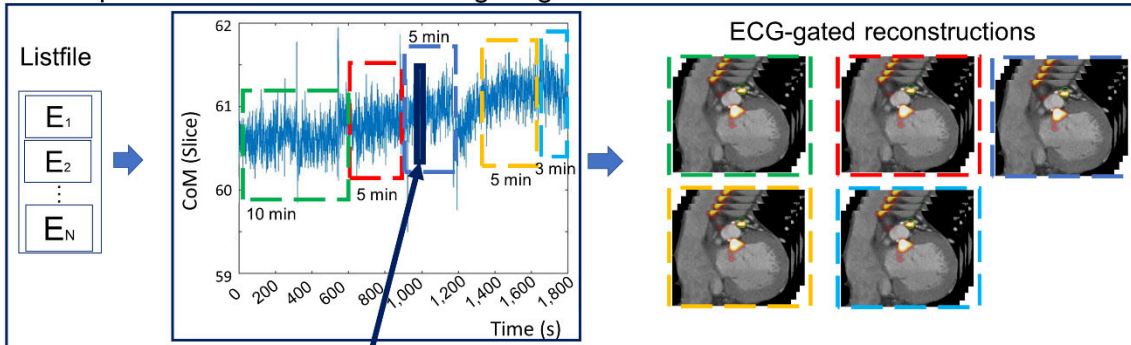
**Table 2:** Maximum standard uptake values (SUV<sub>max</sub>) and target to background (TBR) values observed in the lesions before and after gross patient motion compensation (GPMC). Significant changes are marked in bold.

|                                 | SUV <sub>max</sub> |         |                           | TBR      |         |                              |
|---------------------------------|--------------------|---------|---------------------------|----------|---------|------------------------------|
|                                 | Non-GPMC           | GPMC    | Increase (%)              | Non-GPMC | GPMC    | Increase (%)                 |
| <sup>18</sup> F-NaF-avid (N=38) | 1.8±0.4            | 1.9±0.4 | <b>4.7±5.8 (p=0.0001)</b> | 1.8±0.6  | 2.0±0.7 | <b>8.4±8.6 (p&lt;0.0001)</b> |

**Table 3:** Maximum standard uptake values ( $SUV_{max}$ ) and target to background (TBR) values for  $^{18}F$ -NaF-avid lesions in patients with maximum motion within three intervals (<5, 5-10 and  $\geq 10$  mm). Significant changes are reported in bold.

| Lesions                | $SUV_{max}$   |               |   | TBR           |               |  |
|------------------------|---------------|---------------|---|---------------|---------------|--|
|                        | Non-GPMC      | GPMC          | Increase (%)  | Non-GPMC      | GPMC          | Increase (%)   |
| <5 mm<br>N=8, (21%)    | 1.9 $\pm$ 0.3 | 2.0 $\pm$ 0.3 | 3.5 $\pm$ 5.5<br>(p=0.17)                             | 1.8 $\pm$ 0.2 | 1.9 $\pm$ 0.3 | <b>7.2<math>\pm</math>4.8</b><br>( <b>p=0.003</b> )      |
| 5-10 mm<br>N=15, (38%) | 1.6 $\pm$ 0.4 | 1.7 $\pm$ 0.4 | <b>4.6<math>\pm</math>5.6</b><br>( <b>p=0.02</b> )    | 1.7 $\pm$ 0.3 | 1.8 $\pm$ 0.3 | <b>5.8<math>\pm</math>6.4</b><br>( <b>p=0.002</b> )      |
| >10 mm<br>N=15, (38%)  | 2.0 $\pm$ 0.3 | 2.1 $\pm$ 0.3 | <b>5.0<math>\pm</math>5.3</b><br>( <b>p&lt;0.01</b> ) | 2.0 $\pm$ 0.9 | 2.3 $\pm$ 0.9 | <b>11.5<math>\pm</math>10.1</b><br>( <b>p&lt;0.001</b> ) |

### A Gross patient motion detection and gating



### B

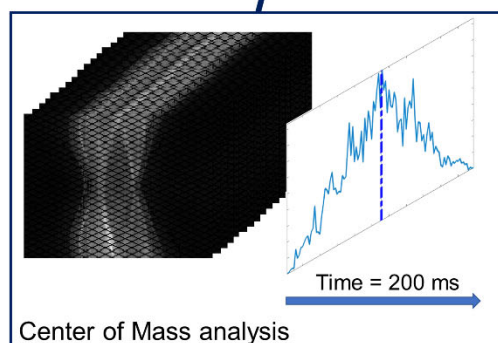
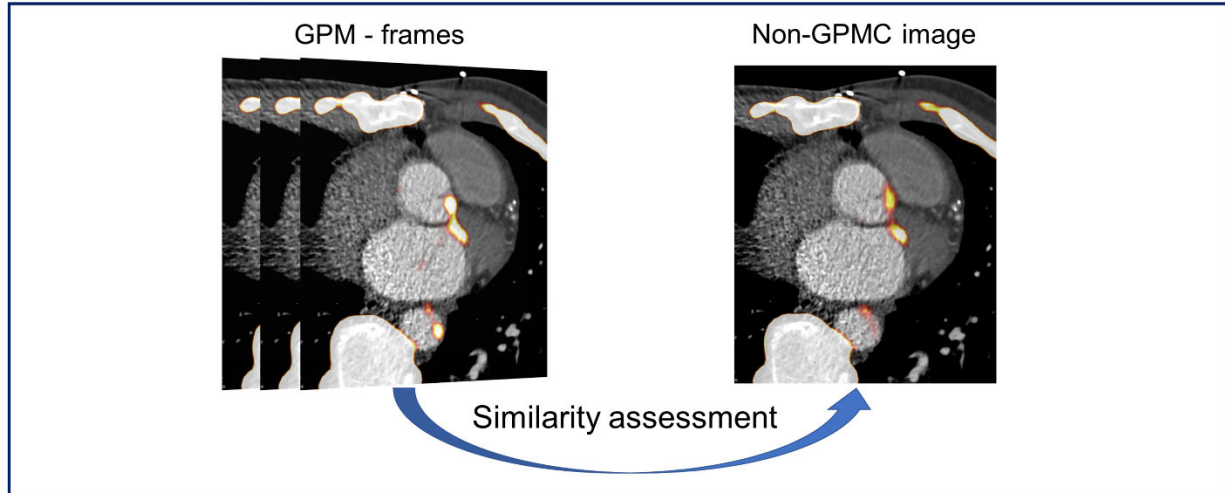


**Figure 1:** Gross patient motion (GPM) detection. **A:** Information on patient repositioning relies on analyses of the events ( $E_1$ - $E_N$ ) stored in the listmode file. **B:** The patient position is obtained for every 200 milliseconds using a Center of Mass (CoM) assessment (Solid dark blue line) of a single-slice rebinned sinogram-series. New GPM frames are defined upon detection of changes in the CoM-baseline ( $>0.5$  mm in 3 seconds, or  $>0.3$  mm over 15 seconds), as exemplified in (**A**) (green, red, dark blue, orange and bright blue dashed frames, respectively).

## Reference gate identification



## Gross patient motion compensation

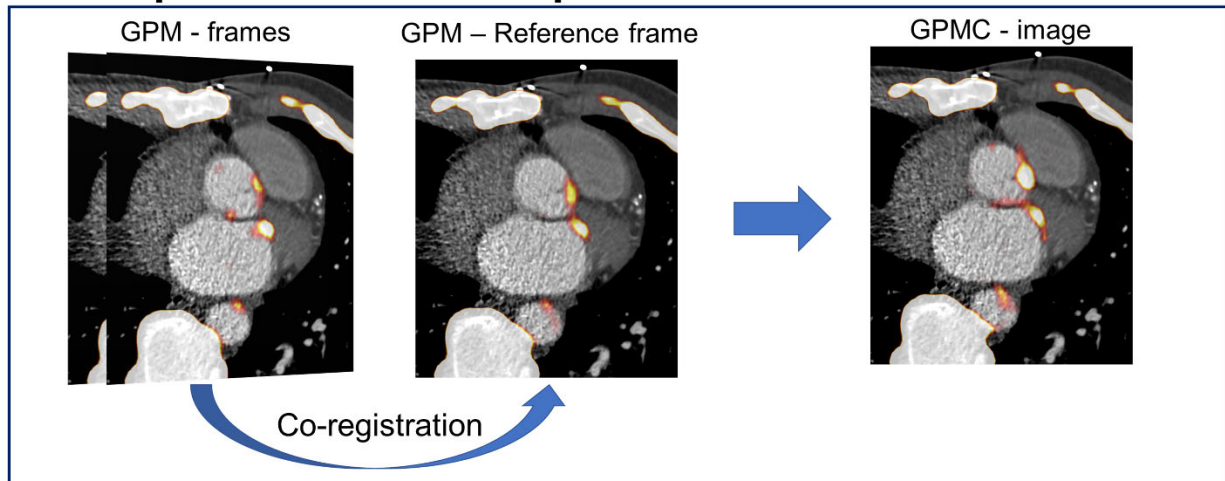


**Figure 2.** Gross patient motion (GPM) compensation (GPMC). The diastolic GPM frames (Figure 1) are compared for similarity with original non-GPMC image. The GPM frame most similar to the original non-GPMC image (top) is chosen as a reference image (most frequently the GPM frame with the longest time-duration). The co-registered images resulted in a gross patient motion compensated (GPMC) image.

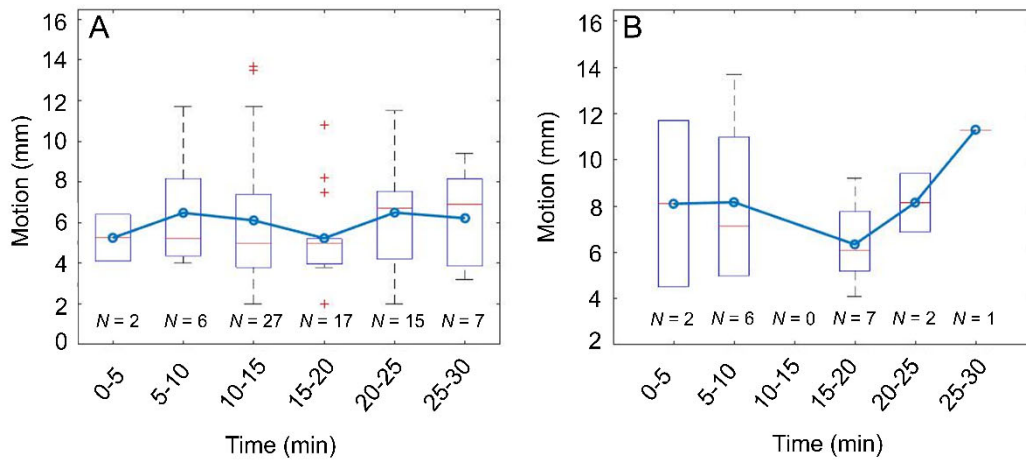


**Figure 3.** Average and maximum (3-dimensional) GPM (gross patient motion) observed in the patients divided into 5-min intervals. **A:** Average GPM observed in all lesions affected by patient repositioning. **B:** Maximal motion throughout the acquisition. Major repositioning events are observed in the beginning and towards the end of the acquisition. Both plots: box-plot and whiskers show median motion (red line), and range in the whiskers while the blue-line with circles connecting the boxes display the mean motion for each time interval.

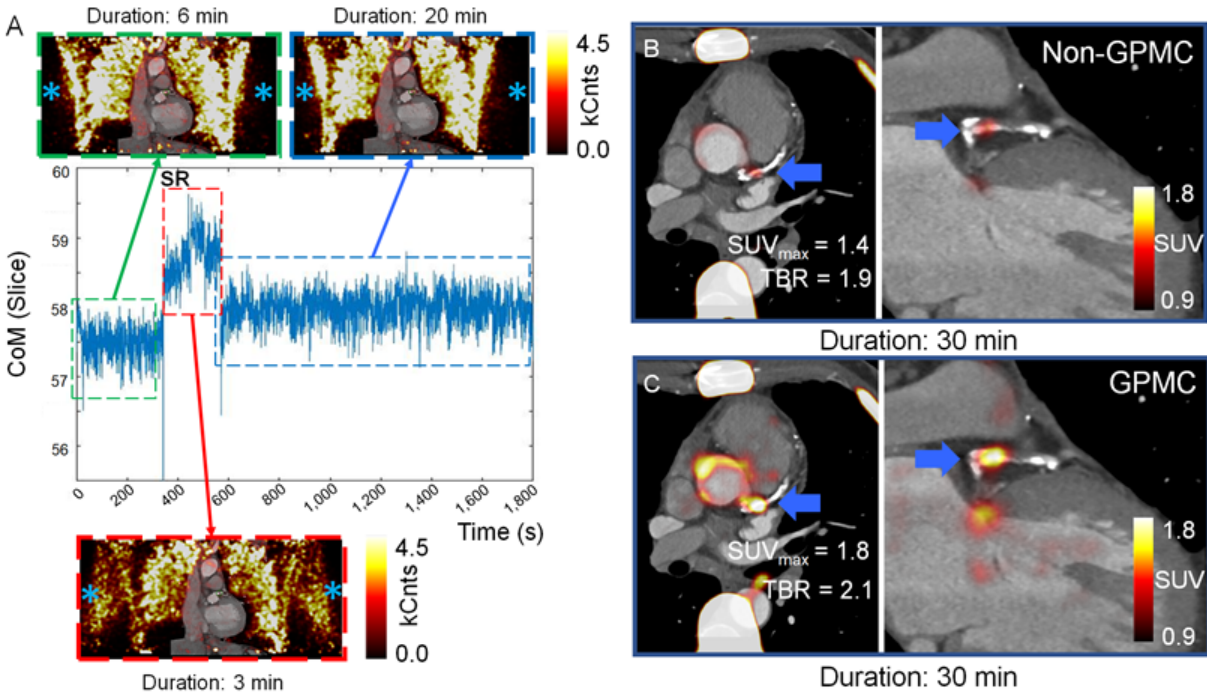


**Figure 4:** Example of a patient with a sudden repositioning (SR) event during the acquisition. The repositioning led to a total of three gross patient motion (GPM) frames (green, red and blue frames, respectively). At minute six, the patient shifted the arms down for a total of 3 minutes (red frame, A), as shown on the non-attenuation corrected images (asterisk, A). The non-attenuation corrected images are not used in the analyses of the patients but are used to visualize repositioning of the arms.

The attenuation corrected PET-images (B and C) represents the standard clinical reconstruction (non-GPMC) and the GPMC datasets, respectively. Compensation of GPM resulted in increased  $SUV_{max}$  and TBR values in the patient (blue arrow, B and C).

### Gross patient motion detection

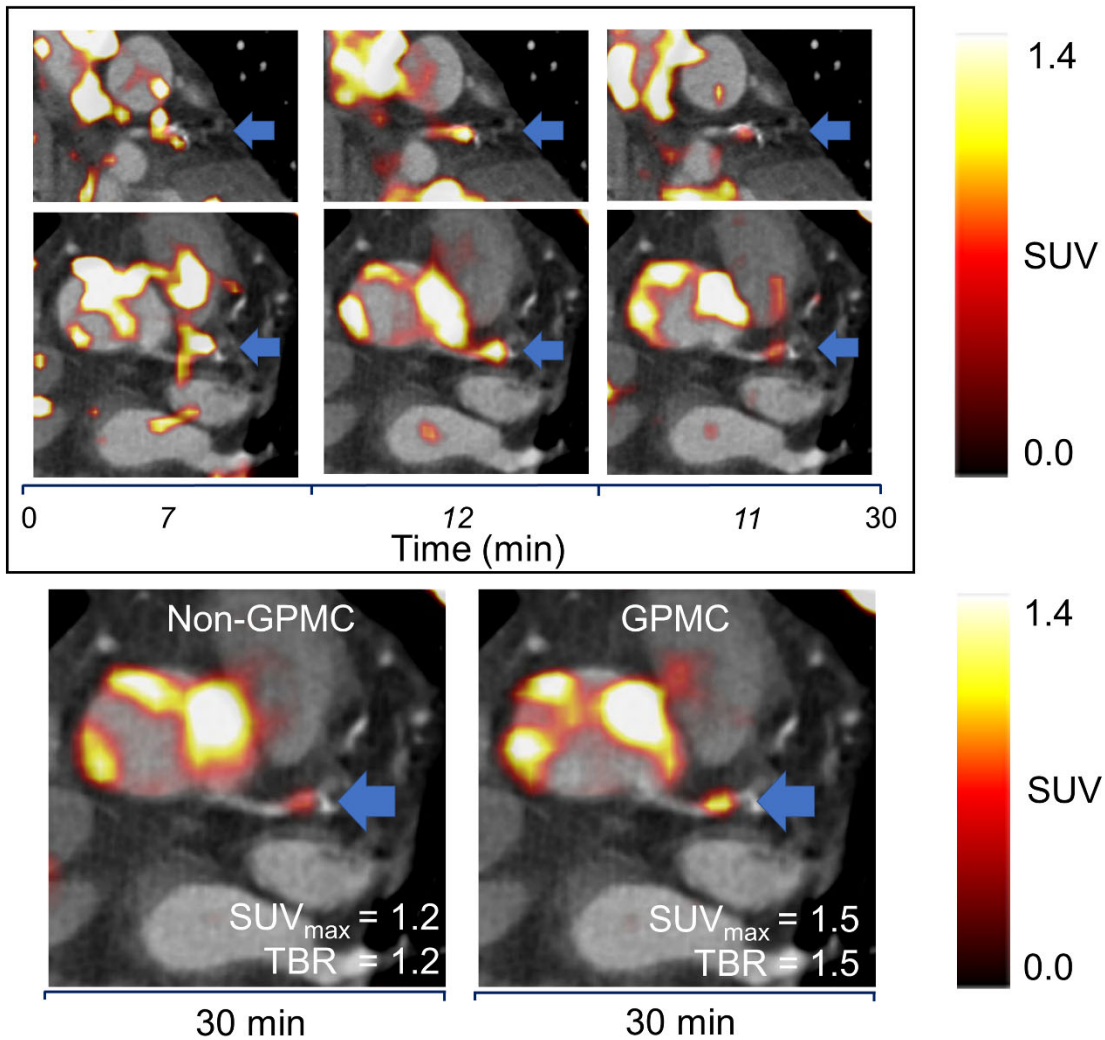


**Figure 5.** An example of a patient with significant motion (11.7 mm) observed during the acquisition. Significant intra-frame motion is observed for the three GPM frames (top). Of note, time in *italic* represents frame-duration and time in **bold** the scan duration. Through co-registration, the lesion activity is increased for the GPMC images, resulting in a transition of the lesion from being  $^{18}\text{F}$ -NaF-negative to be  $^{18}\text{F}$ -NaF avid (bottom). GPM-gross patient motion. GPMC-GPM compensated.

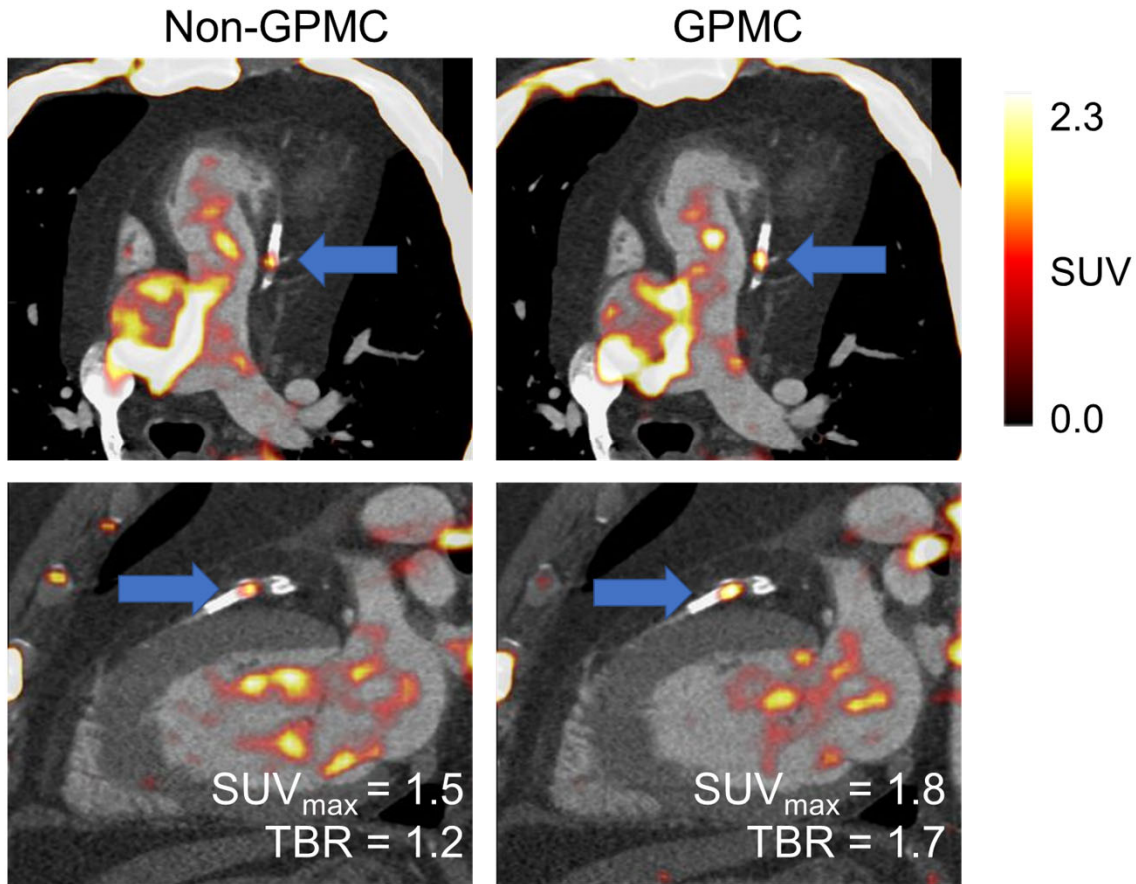


**Figure 6.** Patient with highest increase in the target to background ratio (TBR). Both, the lesion maximum standard uptake value (SUV<sub>max</sub>) and TBR increased significantly on GPMC images (by 20.7% and 40.8%, respectively), leading to the reclassification of the lesion from <sup>18</sup>F-NaF-negative to <sup>18</sup>F-NaF-avid. Of note, the SUV<sub>background</sub> was increased for the Non-GPMC image due to the repositioning events which shifted high activity regions into the volume of interest in the right ventricle. GPMC-gross patient motion compensated.

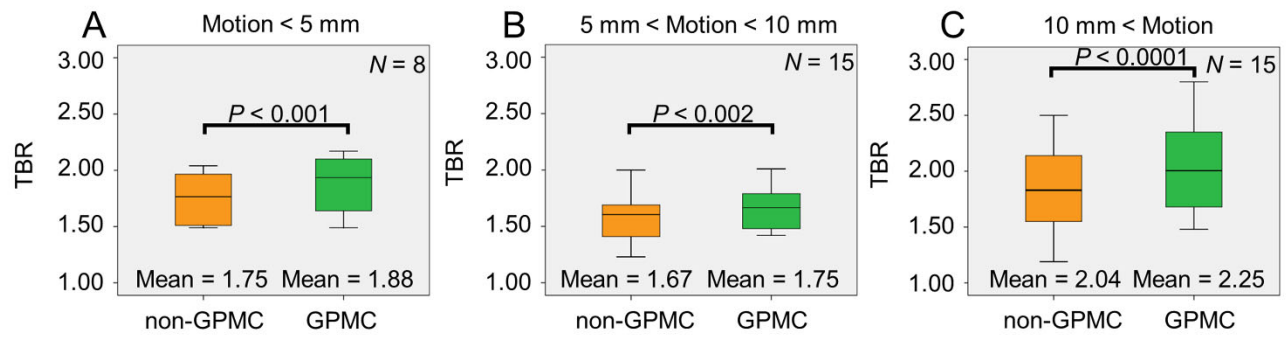


**Figure 7.** Target to background ratios (TBR) in lesions on Non-GPMC and GPMC images. Larger increases in TBR were observed for patients with maximum translations > 10mm. GPMC-gross patient motion compensated.